JOURNAL OF GEOPHYSICAL RESEARCH, VOL. 100, NO. B8, PAGES 15,477–15,488, AUGUST 10, 1995

On the penetration of an endothermic phase transition by upwellings and downwellings

Paul J. Tackley[1]
Seismological Laboratory, California Institute of Technology, Pasadena

Abstract. Using a simple criterion for the deflection of a constant-viscosity upwelling or downwelling by an endothermic phase transition, the scaling of the critical phase buoyancy parameter P_{crit} with the important lengthscales is obtained. The derived trends match those previously observed in time-dependent numerical simulations, implying that geometry is the dominant factor in determining the propensity to layering. For a sinusoidal temperature anomaly, P_{crit} is found to be proportional to wavelength, so that a stronger phase change is required to stop longer wavelengths, in accord with observations from three-dimensional numerical simulations. For more realistic Gaussian upwelling and downwelling features, the dependence of P_{crit} on width of feature, spacing of features, depth of phase transition and width of phase transition are determined for idealized internally heated and basally heated systems. Narrow upwellings and downwellings are deflected more easily than broad ones, providing a first-order explanation for the increased propensity to layering as Rayleigh number is increased. Internal heating is found to strongly favor deflection, particularly when the phase change is at shallow depth. For basally heated systems, the depth of the phase transition is found to be relatively unimportant in determining the value of P_{crit} for which both upwellings and downwellings are deflected. In contrast, for internally heated systems, a shallower phase transition strongly favors layering. Only weak dependence of P_{crit} on the spacing of upwellings and downwellings is found. A narrower phase transition enhances deflection.

Introduction

The ability of an endothermic phase transition at 660 km depth to enforce layered convection in planetary mantles has been the focus of much recent numerical modeling [*Christensen and Yuen*, 1985; *Liu et al.*, 1991; *Machetel and Weber*, 1991; *Zhao et al.*, 1992; *Peltier and Solheim*, 1992; *Weinstein*, 1993; *Honda et al.*, 1993; *Tackley et al.*, 1993, 1994; *Solheim and Peltier*, 1994]. The consensus emerging from these results is that of a partially or intermittently layered mantle characterized by accumulation of cold downwellings above the 660 km discontinuity followed by vigorous, catastrophic "avalanches" of pooled material into the lower mantle. However, despite these recent modeling advances, a theoretical understanding of the important processes is not well developed.

From the numerical experiments, a number of trends are apparent: (1) Flow penetration through the phase transition is strongly wavelength-dependent, with whole-mantle convection observed at long wavelengths (compatible with calculated flow for the Earth [*Phipps Morgan and Shearer*, 1993]), while stratification occurs at short wavelengths [*Tackley et al.*, 1994]. The propensity to layering is increased by (2) increasing the Rayleigh number [*Christensen and Yuen*, 1985; *Solheim and Peltier*, 1994; *Yuen et al.*, 1994], (3) greater internal heating [*Zhao et al.*, 1992; *Solheim and Peltier*, 1994], and (4) narrower phase transitions [*Christensen and Yuen*, 1985; *Peltier and Solheim*, 1992].

There are two dynamical effects associated with phase transitions: the anomalous buoyancy resulting from vertical deflection of the phase boundary, and the latent heat release or absorption [*Schubert and Turcotte*, 1971; *Schubert et al.*, 1975]. At low Rayleigh numbers, latent heat effects are dominant, and for reasonable parameters an endothermic phase transition may be destabilizing, enhancing whole-mantle convection, as demonstrated in early theoretical work involving linear stability analysis [*Schubert and Turcotte*, 1971; *Schubert et al.*, 1975; *Peltier et al.*, 1989]. At higher, more realistic Rayleigh numbers, however, the buoyancy effect is dominant, and an endothermic phase transition favors layered convection. Indeed, *Christensen and Yuen* [1985] demonstrated that latent heat can be ignored to first order at higher Rayleigh numbers. An explanation for this is that in the linear stability analyses, an initially conductive temperature profile is assumed, so that latent heat release or absorption due to movement across the phase boundary results in horizontal temperature differences which drive further flow, although these temperature differences also cause phase boundary deflections which may reduce or even negate the induced flow. The net flow may enhance convection for an endothermic transition but always inhibits convection for an exothermic transition. However, at high Rayleigh numbers, a convective system tends to adopt an adiabatic temperature stratification. In this case, the temperature change due to

[1]Now at Department of Earth and Space Sciences, University of California Los Angeles.

Paper number 95JB00318
0148-0227/95/95JB-00318$05.00

latent heat can be considered as adiabatic (reasonable because convective velocities are very much larger than the characteristic diffusion velocity κ/D, where κ is the thermal diffusivity and D is the depth of layer). Hence the temperature offset due to latent heat occurs along the entire phase boundary, and movement through the phase transition does not result in additional horizontal temperature gradients. Thus it is reasonable to focus exclusively on buoyancy effects due to deflection, when analyzing the effects due to phase transitions at high Rayleigh numbers.

In order to analyze the interaction of convective upwelling or downwellings with an endothermic phase transition, three distinct stages or regimes can be identified, which are sketched in Figure 1. (1) (Figure 1a) An upwelling or downwelling reaches the phase transition: does it penetrate or get deflected? (2) (Figure 1b) If deflected, deflected material pools above (for a downwelling) or below (upwelling) the phase transition, until the pool reaches a sufficient size to break through. This regime has been analyzed for the case of highly viscous downwellings by *Bercovici et al.* [1993], who find that cylindrical and linear downwellings are fundamentally different in their penetrative behavior. (3) (Figure 1c) If pooling of material is pervasive, an internal boundary layer builds up: when does breakdown of layering occur? This regime has been studied by applying a local boundary layer analysis to the internal boundary layer to predict when it will become unstable, and hence breakthrough will occur [*Solheim and Peltier*, 1994], which results in a periodicity with a distinct timescale.

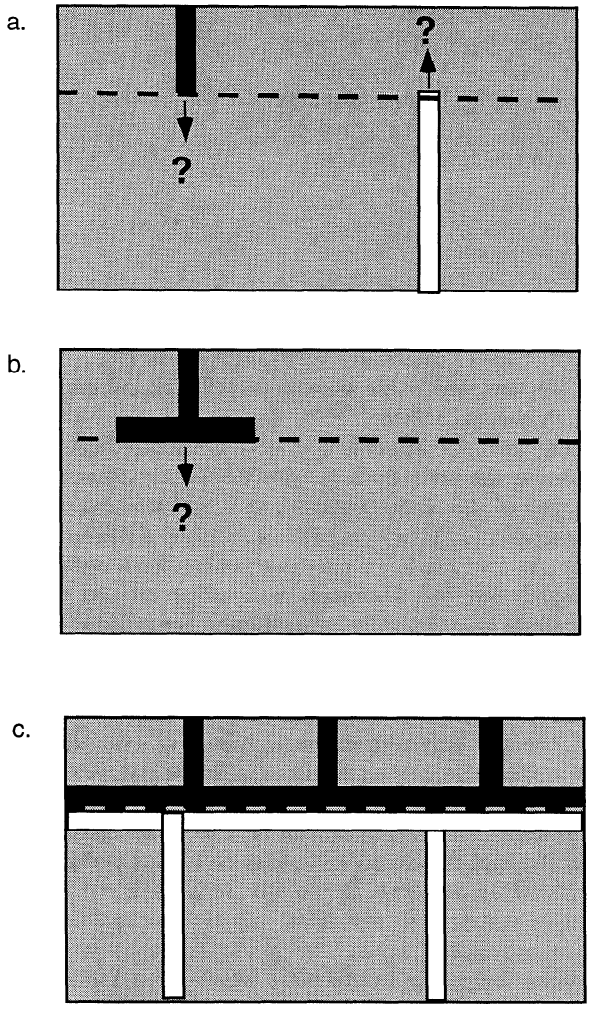

Figure 1. The three stages/regimes of behavior, in the interaction of convective features with an endothermic phase boundary. Black features are cold downwellings, white features are hot upwellings. (a) Upwellings and downwellings first meet the phase transition. (b) Pooling of a downwelling above the phase transition. (c) Pervasive layering.

Although the second and third regimes have received recent attention, the first regime, shown in Figure 1a, has not. *Yuen and Olson* [1982] presented some analytical calculations for a plume encountering phase transitions and concluded that the Clapeyron slope of the transition must exceed -30 MPa K^{-1} to prevent penetration. Later numerical simulations, however, indicated that a much lower value of -6 MPa K^{-1} could enforce total layering [*Christensen and Yuen*, 1985], with strongly intermittent layering occurring at lower values such as -2 MPa K^{-1} [*Machetel and Weber*, 1991], or -2.8 MPa K^{-1} [*Peltier and Solheim*, 1992]. The purpose of this present study is to examine this regime in detail, by means of analytic models in which the interaction of idealized upwellings and downwellings with an endothermic phase change is examined and the effect of the important length scales is determined. Since this paper considers only the initial deflection or penetration of an upwelling or downwelling, and not their ponding at the phase boundary, the results represent the threshold between straight penetration of upwellings and downwellings and an intermittent regime with ponding and avalanches.

Model

Two-dimensional Cartesian geometry is assumed for this present study. The use of three-dimensional and/or spherical geometry will probably change the quantitative nature of the results, but not the observed trends, which are the main focus of this study. The Boussinesq approximation is assumed in this two-dimensional Cartesian geometry, allowing a simple streamfunction formulation of the governing equations [e.g., *Turcotte and Schubert*, 1982].

$$\nabla^4 \psi = \rho_{,x} \tag{1}$$

$$u = -\psi_{,z} \quad ; \quad v = \psi_{,x} \tag{2}$$

where Ψ is the stream function, ρ is the nondimensional density (representative of buoyancy), and u and v are horizontal and vertical nondimensional velocities, respectively. The conventional nondimensionalization to thermal scales is assumed, that is, velocity to κ/h, and density perturbation to $\eta\kappa/(gh^3)$, where κ is the thermal diffusivity, h is the depth of layer, η is the dynamic viscosity, and g is the gravitational acceleration.

The anomalous buoyancy resulting from phase boundary deflection is represented as a mass anomaly at a prescribed depth (discontinuous phase transition) or depth range (finite width phase transition). This is equivalent to the sheet mass anomaly approach of *Tackley et al.* [1993, 1994] (discontinuous phase transition) or the effective thermal expansivity approach of *Christensen and Yuen* [1985] (finite width phase transition), both of which have been found in numerical simulations to give a reasonable approximation to a

full treatment when phase boundary deflection is small compared to the width of convective features. When phase boundary deflection becomes comparable to width of convective features, this approximation become inaccurate. However, since the aim of this study is to establish trends and to derive simple scaling relationships, this seems a reasonable approximation at this stage.

The effect of the phase transition is represented by a single parameter, the phase buoyancy parameter P, which can be interpreted as the ratio of buoyancy due to phase change deflection to the buoyancy due to thermal effects, integrated over a column:

$$\sigma_{phase} = \delta_{ph}\Delta\rho_{ph} = \frac{\gamma\Delta T}{\rho g}\Delta\rho_{ph} \tag{3}$$

$$\sigma_{thermal} = \rho g \alpha \Delta T h \tag{4}$$

$$P = \frac{\sigma_{phase}}{\sigma_{thermal}} = \frac{\gamma\Delta\rho}{g\alpha\rho^2 h} \tag{5}$$

where σ_{phase} and $\sigma_{thermal}$ are the anomalous surface densities (i.e., mass per unit area) due to phase change deflection and thermal expansion respectively, δ_{ph} is the phase change deflection, γ is the Clapeyron slope, $\Delta\rho_{ph}$ is the density jump across the phase change, g is gravitational acceleration, α is thermal expansivity, ΔT is a temperature scale (usually taken to be the superadiabatic temperature drop across the layer), and h is a length scale (usually taken to be the depth of the layer). It is important to note that the influence of the phase transition is independent of temperature scale, since both phase change deflection and thermal buoyancy are proportional to temperature. Representative values of the relevant parameters are listed in Table 1. The phase buoyancy parameter resulting from these is of order -0.1.

The analysis starts with the simplest possible case and progresses through models of increasing realism as follows:

1. We examine analytically the interaction of a sinusoidal temperature anomaly with an endothermic phase change separating two infinite half-spaces. This regime is relevant to a local analysis around the phase change region, when the effects of upper and lower boundary conditions are not significant. Information about the wavelength dependence of flow penetration, and the scaling of critical phase buoyancy parameter with wavelength, is obtained.

2. Upper and lower boundary conditions are added, and the analysis for a sinusoidal temperature anomaly is repeated. Additional information about the effect of boundaries, phase change depth, and phase change width, is obtained.

3. More realistic upwellings and downwelling are considered, assuming a Gaussian horizontal temperature profile. The effect of the important length scales, namely, width of feature, spacing of features, depth of phase transition, and width of phase transition, are obtained. Convective features which have just reached the phase boundary, as well as those which extend throughout the mantle depth, are considered.

Table 1. Representative Values of Parameters at the 660-km Discontinuity

Symbol	Parameter	Value	Units
γ_{660}	Clapeyron slope at 660 km	-3	MPa K^{-1}
$\Delta\rho_{660}$	density jump at 660 km	400	kg m^{-3}
g_{660}	gravitational acceleration	9.8	m s^{-2}
α_{660}	thermal expansivity	2.5×10^{-5}	K^{-1}
ρ_{660}	mean density	4200	kg m^{-3}
h	mantle depth	2890	km
P_{660}	phase buoyancy parameter	-0.096	-

Results

Infinite Domain, Sinusoidal Anomaly

The flow solution for a horizontally sinusoidal temperature anomaly in an infinite domain with a phase transition can be obtained straightforwardly using a Fourier transform method. First (1) is transformed into Fourier space:

$$(k^2 + l^2)^2 \tilde{\psi} = ik\tilde{\rho} \tag{6}$$

$$\tilde{\psi} = \frac{ik\tilde{\rho}}{(k^2 + l^2)^2} \tag{7}$$

where k and l are the horizontal and vertical wave numbers, respectively, and ρ is density. Thus the different flow solutions can be obtained by inserting appropriate density anomalies into the above equation.

Density function. Consider a periodic nondimensional temperature distribution with wavenumber k_0. For algebraic simplicity we will use the form $\exp(ikx)$, bearing in mind that the physically observable component corresponds to the real part of this.

$$T = T_0 \exp(ik_0 x) \tag{8}$$

$$\rho = \rho_0 - Ra.T = \rho_0 - Ra.T_0 \exp(ik_0 x) \tag{9}$$

where ρ_0 is the nondimensional background density and the Rayleigh number (Ra) is defined in terms of previously defined parameters plus the (dimensional) mantle density ρ_m as

$$Ra = \frac{\rho_m g \alpha \Delta T h^3}{\eta\kappa}. \tag{10}$$

This periodic temperature anomaly induces a periodic sheet mass anomaly at the phase change depth (z=0) given by

$$\sigma = -P.Ra.T \tag{11}$$

giving a total density function

$$\rho = \rho_0 - Ra.T_0\left[1 + P\delta(z)\right]\exp(ik_0 x)\,. \tag{12}$$

Transforming into Fourier space (where the $1/(2\pi)^2$ normalization is applied entirely on the forward transform);

$$\tilde{\rho} = \rho_0\delta(k)\delta(l) - Ra.T_0\delta(k-k_0)\left[\delta(l) + \frac{P}{2\pi}\right] \tag{13}$$

and substituting into (7) yields a spectral flow solution:

$$\tilde{\psi} = -iRaT_0\delta(k-k_0)\left[\frac{\delta(l)}{k_0{}^3} + \frac{k_0 P}{2\pi(k_0^2+l^2)^2}\right]. \quad (14)$$

Noting that

$$IFT_\ell\left(\frac{k_0}{(k_0^2+l^2)^2}\right) = \frac{\pi}{2k_0^2}[1+k_0|z|]\exp(-k_0|z|) \quad (15)$$

where IFT ℓ denotes inverse Fourier transform in ℓ, valid for $k_0>0$ (this result was derived from Fourier transform pairs 7 and 9 of *Gradshteyn and Ryzhik* [1980, p1147]), we obtain

$$\psi = -\frac{iRaT_0}{k_0^2}\left[\frac{1}{k_0} + \frac{P}{4}(1+k_0|z|)\exp(-k_0|z|)\right]\exp(ik_0x) \quad (16)$$

giving a vertical velocity

$$v = \psi_{,x} = \frac{RaT_0}{k_0}\left[\frac{1}{k_0} + \frac{P}{4}(1+k_0|z|)\exp(-k_0|z|)\right]\exp(ik_0x) \quad (17)$$

Critical parameters. The vertical velocity across the phase change (at z=0) is given by

$$v(x,0) = \frac{RaT_0}{k_0}\left[\frac{1}{k_0} + \frac{P}{4}\right]\exp(ik_0x). \quad (18)$$

Thus by requiring $v(x,0)$=0, the critical phase buoyancy parameter for inhibition of flow of wavelength λ across the phase transition is obtained.

$$P_{crit} = -(2/\pi)\lambda \quad (19)$$

Alternatively, the critical wavelength, below which flow will be inhibited by a phase change of strength P, and above which flow will penetrate, is given by

$$\lambda_{crit} = -(\pi/2)P. \quad (20)$$

So there is a straightforward proportionality between P_{crit} and λ. This is easy to understand since in this case there is only one lengthscale, the horizontal wavelength, and thus a self-similar solution is expected, dependent on the single parameter λ/P. This relationship provides a first-order explanation of the observation made by *Tackley et al.* [1994], that flow at long wavelengths tends to penetrate the phase transitions whereas flow at short wavelengths tends to be inhibited from penetrating.

Note that shorter wavelengths, or stronger P, would imply a total vertical velocity (at z=0) in the opposite direction to thermally driven flow. However, a real, thermally driven convective system would be unable to reach a point at which local phase-change driven flow exceeded local thermally driven flow, since it would first have to pass through a point at which the two were equal, implying zero vertical velocity. The system would adjust itself so that $v_z(x,0)$=0 for wavelengths less than the critical. For P=-0.1, the representative value from Table 1, the critical nondimensional wavelength is 0.157, corresponding to a dimensional wavelength of 454 km.

Bounded Domain, Periodic *T*

It is desirable to determine the effect of boundaries on the above solution, and for this purpose, impermeable, free-slip boundaries are imposed at z=0 (lower boundary) and z=1 (upper boundary), with the phase change occurring at a distance d_{ph} from the upper boundary, that is, at z=1-d_{ph}. A sinusoidal temperature anomaly, independent of z, is imposed, as before. Note that this is not the temperature field of thermal convection, which normally has constant temperature boundary conditions, but it can be thought of as a realisitic Fourier decomposition of the temperature field everywhere except in the boundary layers. At this point the effect of finite width phase boundary (as opposed to discontinuous) is also investigated, leading to four parameters: the horizontal wavelength λ, the phase buoyancy parameter P, the depth of the phase change d_{ph}, and the half width of the phase change w_{ph}.

The velocity solution is obtained numerically using the spectral technique described in the appendix. A numerical

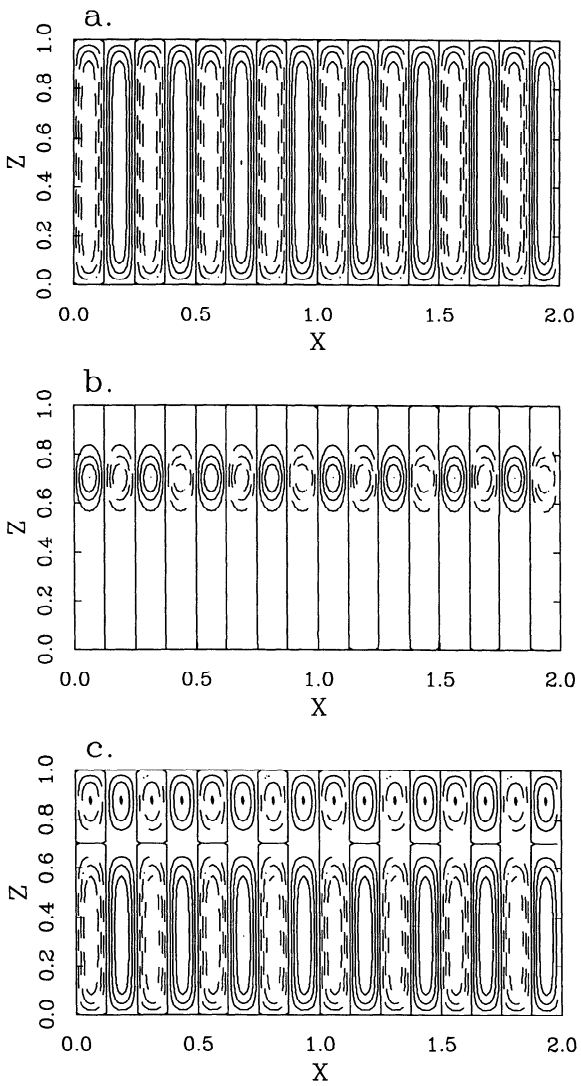

Figure 2. Flow fields (stream function) for a short-wavelength sinusoidal temperature field (wavelength is 0.25). (Top) Thermally driven flow, (middle) phase-change driven flow, and (bottom) total flow for critical phase buoyancy parameter. Note how the phase-change driven flow is localized around the phase transition for this wavelength.

rather than analytical technique is used for flexibility, although for the simplest cases considered, an analytical solution may be possible. In cases with a finite width phase transition, a tanh profile describes the transition from one phase to the other, leading to a phase-change effective thermal expansivity [*Christensen and Yuen*, 1985] as given below:

$$\alpha_{phase}(d) = \frac{P}{2w_{ph}}\left(1-\tanh^2\left[\frac{d-d_{ph}}{w_{ph}}\right]\right) \qquad (21)$$

where d is depth, and w_{ph} is half width of phase transition. Figures 2 and 3 show flow solutions for short and long horizontal wavelengths, respectively. In each case the critical phase bouyancy parameter has been chosen for the total solution. For the shorter wavelength, the phase-change driven flow (Figure 2b) is localized around the phase boundary; away from the phase boundary, the total solution (Figure 2c) resembles the thermally driven solution (Figure 2a). For the long wavelength temperature field, however, both thermally driven flow (Figure 3a) and phase-change driven flow (Figure 3b) fill the domain. This indicates that the vertical extent of flow caused by a sheet mass anomaly is comparable to the horizontal wavelength of the sheet mass anomaly, as is evident from (19).

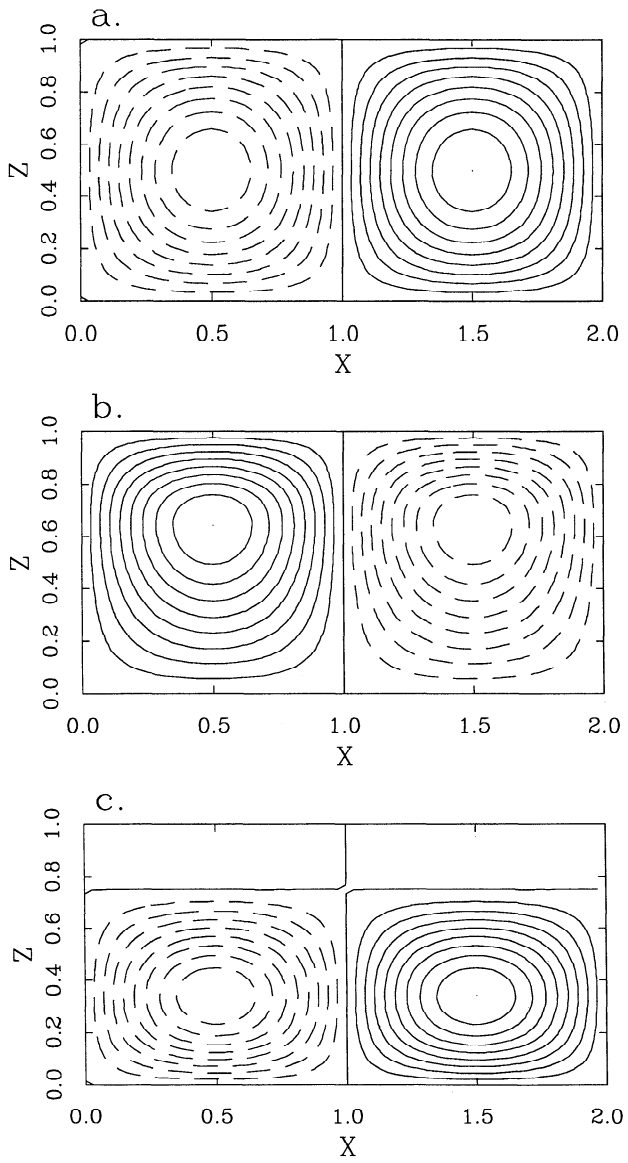

Figure 3. Flow fields (stream function) for a long-wavelength sinusoidal temperature field (wavelength=2.0). (Top) Thermally driven flow, (middle) phase-change driven flow, and (bottom) total flow for critical phase buoyancy parameter. Note how the phase-change driven flow extends throughout the domain for this wavelength.

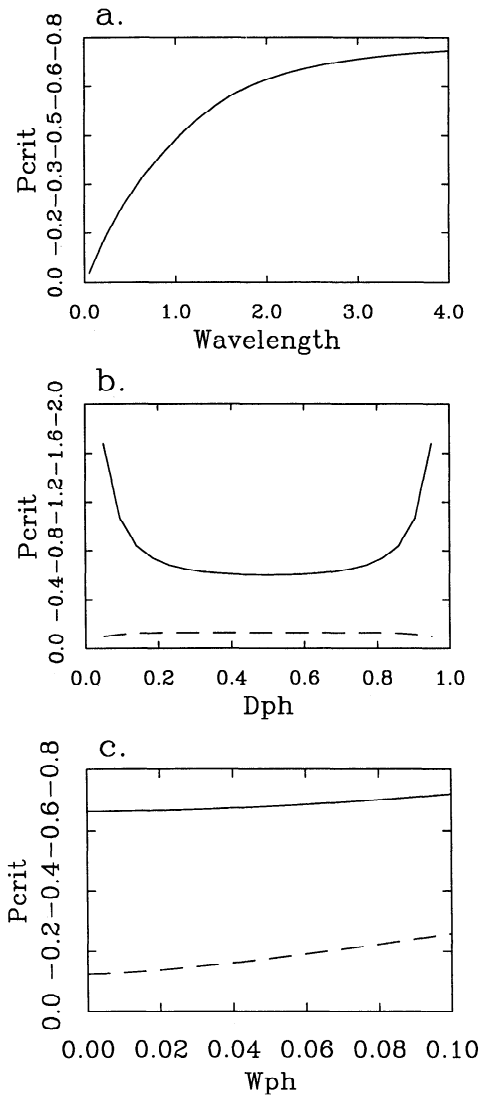

Figure 4. Critical phase buoyancy parameter (P_{crit}) plotted against the three important lengthscales, for a sinusoidal temperature field in a bounded domain. The two curves in Figures 4b and 4c refer to short (0.2, dashed line) and long (2.0, solid line) wavelengths.

The dependence of P_{crit} on the three important lengthscales is given in Figure 4. For each graph, the other lengthscales are set to the default values given in Table 2. Figure 4a gives the dependence of P_{crit} on the horizontal wavelength, nondimensionalized to the depth of the box. At short wavelengths the slope of the graph is approximately $(2/\pi)$, consistent with the analytical solution derived earlier. At these wavelengths, the effects of boundaries are negligible and it is

Table 2. Default Values of Length Scales

Symbol	Meaning	Default Value
λ or L_x	wavelength	2.0
d_{ph}	phase transition depth	0.25
w_{ph}	phase transition half width	0.0
w_x	half width of upwelling and downwelling	0.01

reasonable to assume an infinite domain when calculating flow close to the phase boundary. However, as the wavelength is increased, the boundaries become increasingly important and the gradient of the curve decreases greatly, thereby reducing P_{crit} from the infinite domain solution. The boundary conditions reduce the strength of phase transition required to prevent flow from penetrating, particularly at long wavelengths.

The effect of phase transition depth is illustrated in Figure 4b, for two wavelengths, 0.25 and 2.0. Over a depth range of approximately 0.2 to 0.8, the depth of the phase change has very little influence on P_{crit}. However, when the phase transition is very close to the boundary, the required phase change strength can change greatly.

The width of the phase transition is varied in Figure 4c, for the same two wavelengths. At the longer wavelength of 2.0, the required value of $|P_{crit}|$ increases slightly as the width of phase transition in increased to 0.1. However, for the shorter wavelength of 0.25, there is a large increase in $|P_{crit}|$, approximately doubling from around 0.13 to 0.26. Thus a wider phase transition region decreases the ability of a phase transition to stop flow, particularly when the wavelength is comparable to the width of the phase transition, implying that the short wavelengths which are most likely to be inhibited are also the most sensitive to the width of the phase transition. This is in accordance with the two-dimensional numerical simulations of *Christensen and Yuen* [1985] and *Peltier and Solheim* [1992] and illustrates the importance of trying to obtain a phase transition width as narrow as possible. The phase transition width for the Earth is expected, from laboratory experiments [*Ito and Takahashi*, 1989] and seismological observations [*Benz and Vidale*, 1993] to be a few kilometers at most.

Given that P at the 670-km phase transition is of order -0.1, as shown earlier, only the shortest wavelengths are likely to be completely inhibited from crossing the phase transition, assuming a constant amplitude with depth. However, if long-wavelength temperature anomalies have a peak near 660 km depth, as indicated in the numerical solutions, then these modes will be more inhibited than predicted here.

Gaussian Upwellings and Downwellings

Convective features in real systems do not in general resemble sine waves, and thus it is desirable to consider the interaction of more realistic upwellings and downwellings with phase transitions. In constant-viscosity simulations, the upwellings and downwellings have an approximately Gaussian temperature profile, the profile that is chosen here. Four idealized scenarios are considered, as illustrated in Figure 5. These span the extremes of complete basal heating, represented by an upwelling and a downwelling of equal strength and width, and internal heating, in which only downwellings are present. Of course, these are only crude

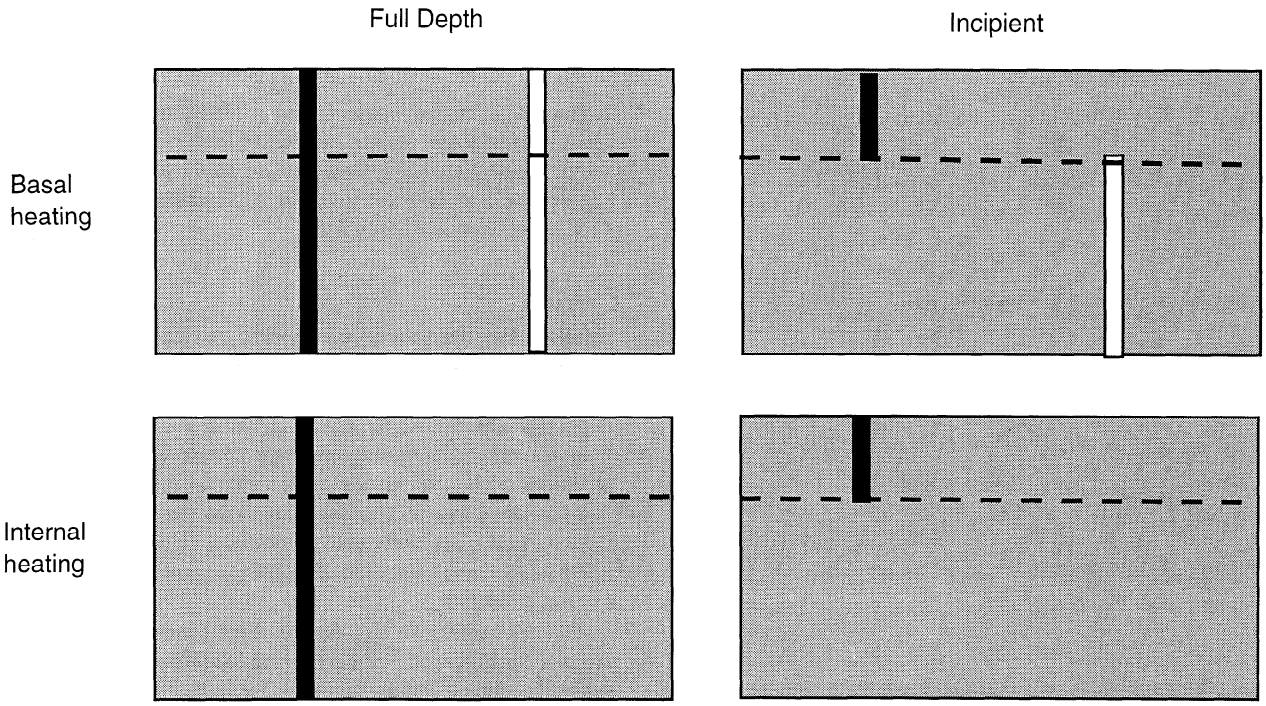

Figure 5. Idealized upwellings and downwellings for the four cases analyzed. Black features are cold downwellings, and white features are hot upwellings. (Top) Basally heated cases, and (bottom) internally heated cases. (Left) Upwellings and downwellings extending through the full depth of the box, and (right) upwellings and downwellings just reaching the phase transition.

approximations of real convective systems, which may have long wavelength anomalies in addition to concentrated features, but are useful for establishing some first-order trends. Initially, we consider upwellings and downwellings which extend the depth of the box, as by *Yuen and Olson* [1982]. Since we are, however, interested in determining whether an upwelling or downwelling that has just reached the phase change will penetrate, we then progress to cases in which the upwellings and downwellings have just reached the phase transition.

An additional length scale, the width of convective feature, is introduced, leading to a total of four lengthscales: the horizontal periodicity (L_x), depth of phase transition (d_{ph}), half width of phase transition (w_{ph}) and width of convective feature (w_x). Default values of these are listed in Table 2. The numerical technique is that used in the previous section and described in the appendix. In these results, w_x is defined as the Gaussian half width of the temperature anomaly, that is, the temperature profile through an upwelling or downwelling is given by

$$\Delta T \propto \exp\left[-\left(\frac{x-x_0}{w_x}\right)^2\right]. \qquad (22)$$

A typical flow pattern for the case of basal heating and upwellings and downwellings extending the full height of the box (as illustrated in Figure 5a) is given in Figure 6. The total solution has $P=P_{crit}$, which is here defined as the value required for zero velocity in the center of the upwelling or downwelling. However, away from the upwelling or downwelling, flow penetrates the phase transition, a phenomenon which can be seen in the numerical results of *Weinstein* [1993]. It is only in regions where temperature anomalies exist at 660 km that flow is inhibited from crossing the phase transition.

Figure 7 shows the results for the case of basal heating with Gaussian upwellings and downwellings extending the full height of the box (as illustrated in Figure 5a). The trends of P_{crit} with w_{ph} (Figure 7a) and d_{ph} (Figure 7b) are similar to those observed with the sinusoidal anomaly: increased phase transition thickness increases P_{crit}, and phase change depth does not have much effect except when the phase transition is near one of the boundaries. The trends of P_{crit} with w_x and L_x are new. P_{crit} increases as the width of upwelling or downwelling increases, so that for a fixed P, narrow features are deflected whereas broad features will penetrate. The horizontal spacing of features (L_x) does not have much effect, except for very small spacing, at which deflection of upwellings and downwellings becomes easier.

With internal heating (graphs in Figure 8, illustration in Figure 5c), similar trends are observed, except that values of P_{crit} are lower, implying that internal heating increases the propensity to layering.

When upwellings and downwellings that have just reached the phase transition are considered (graphs in Figure 9, illustrated in Figure 5b), the trends are similar to the case with full-length upwellings and downwellings, but a number of differences arise. First, when the phase transition is not at mid depth, a different strength is required to stop the upwelling than to stop the downwelling, as indicated by the two curves in each part of Figure 9. When the phase change is at shallow depth, the upwelling can penetrate more easily than the downwelling, as observed in the numerical simulations of

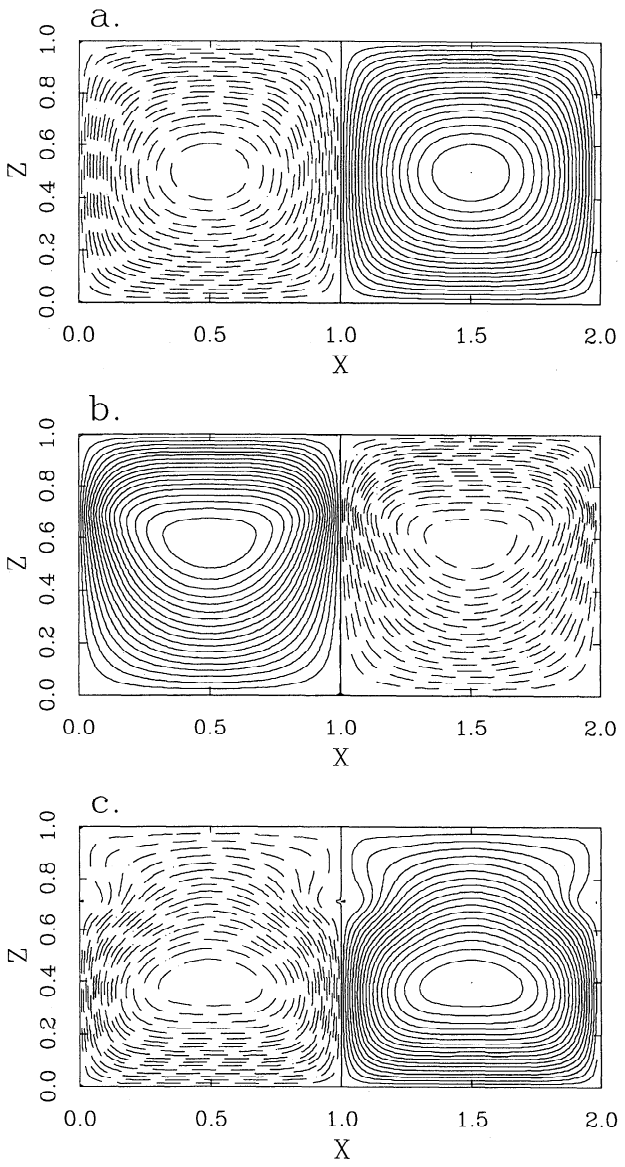

Figure 6. Flow field for full depth, basally heated case. Upwelling at x=0, x=2 and downwelling at x=1.0. Note that away from the upwellings and downwellings, flow penetrates the phase transition.

Tackley et al [1993, 1994]. This may be because the upwelling has a longer buoyant column than the downwelling. Second, the values of P_{crit} are significantly lower. This is due to the fact that the phase-change deflection and hence buoyancy is the same, but depth-integrated thermal buoyancy is reduced since the features do not extend through the whole depth of the box.

For internal heating and downwellings that have just reached the phase change (graphs in Figure 10, illustrated in Figure 5d), similar trends are observed but the following differences arise. First, the depth of the phase transition becomes very important, with deflection becoming easier for shallower phase changes, and more difficult for deeper phase changes. Second, the value of P_{crit} is much lower for internal heating than that for basal heating, a result which has been observed in numerical simulations [e.g., *Solheim and Peltier*, 1994].

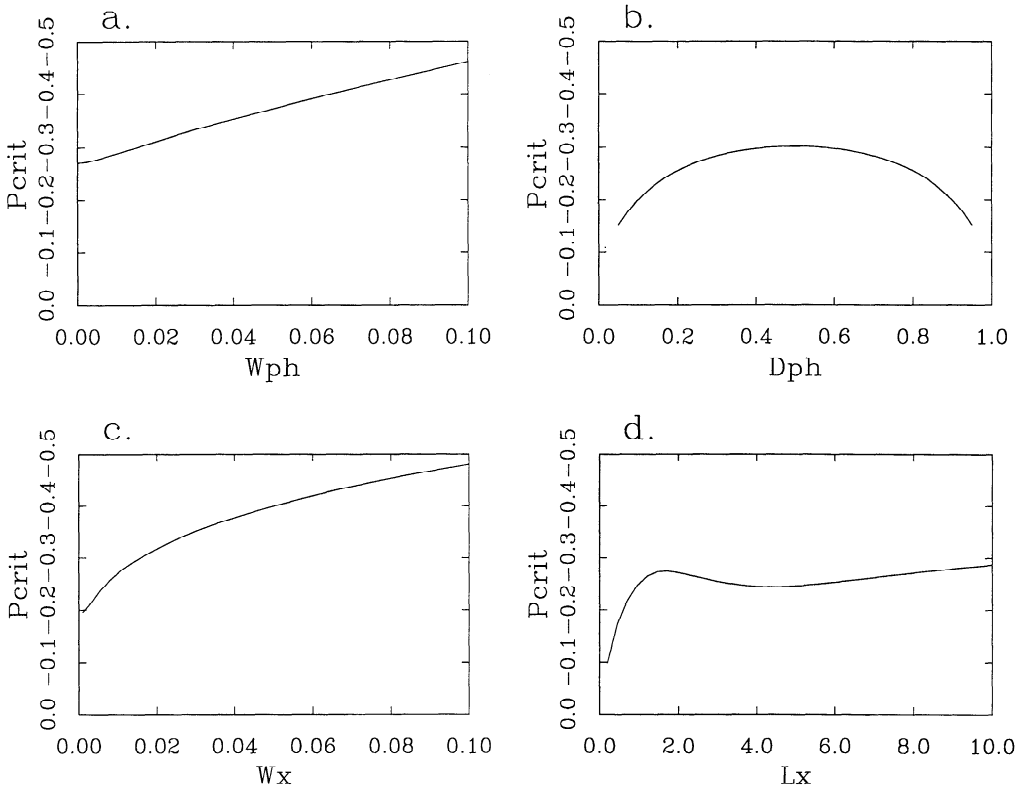

Figure 7. Critical phase buoyancy parameter P_{crit} plotted against the four important lengthscales, for basally heated convection with upwellings and downwellings extending throughout the entire domain (Figure 5a).

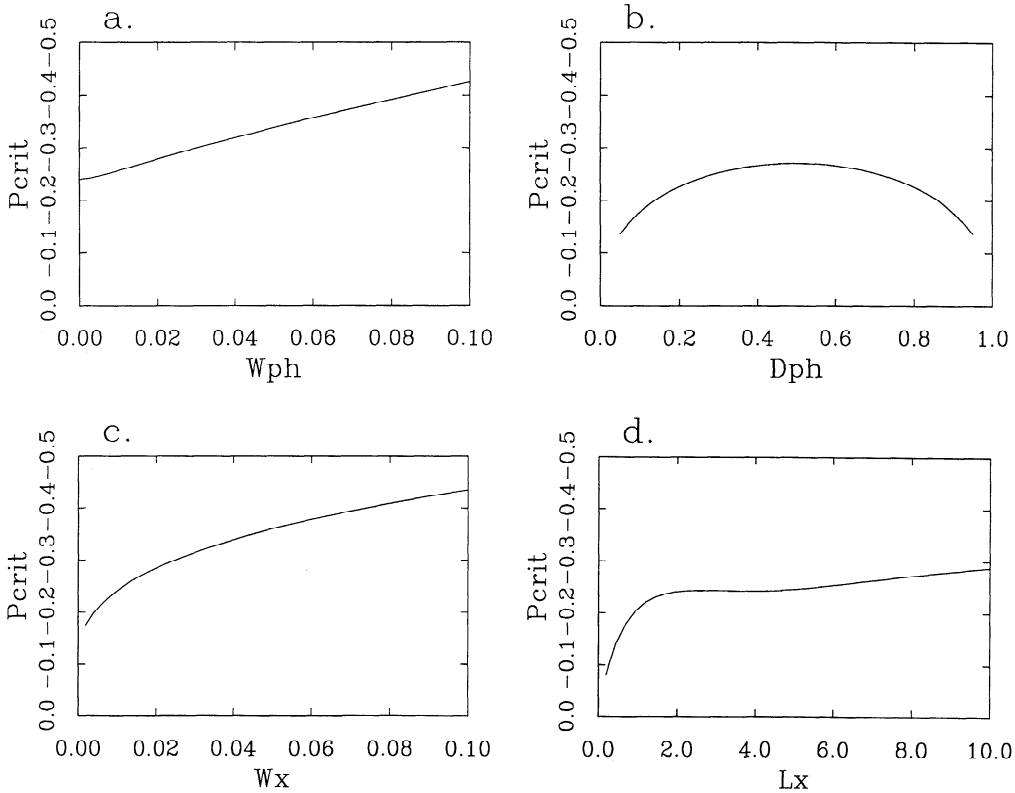

Figure 8. Critical phase buoyancy parameter P_{crit} plotted against the four important length scales, for internally heated convection with downwellings extending throughout the entire domain (Figure 5c).

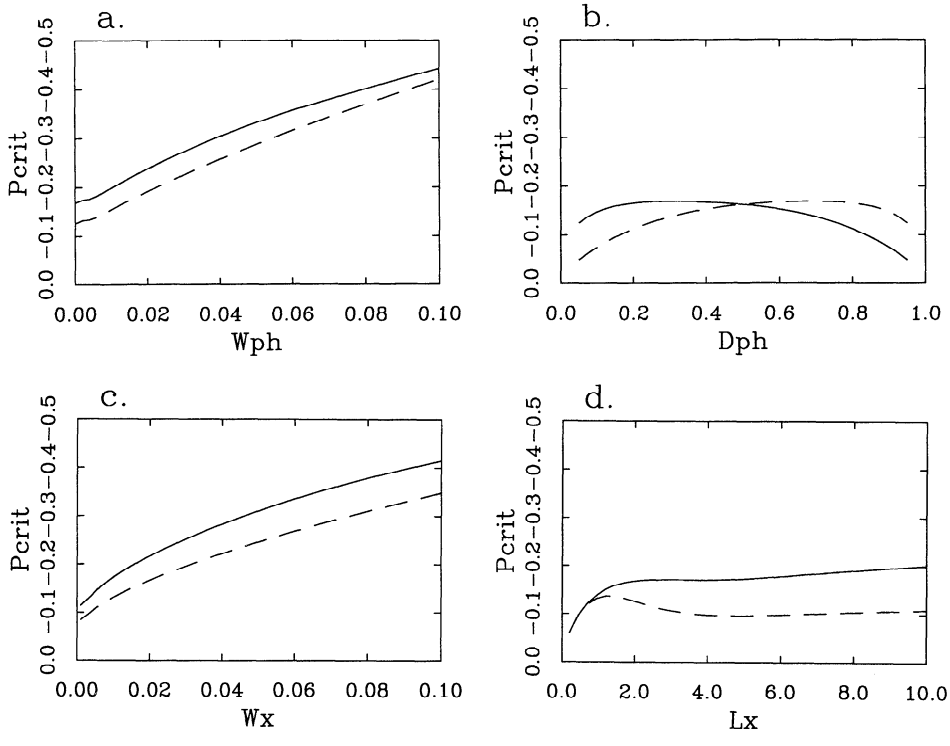

Figure 9. Critical phase buoyancy parameter P_{crit} plotted against the four important length scales, for basally heated convection with upwellings and downwellings just reaching the phase transition (Figure 5b). Solid lines are for upwellings, dashed lines for downwellings.

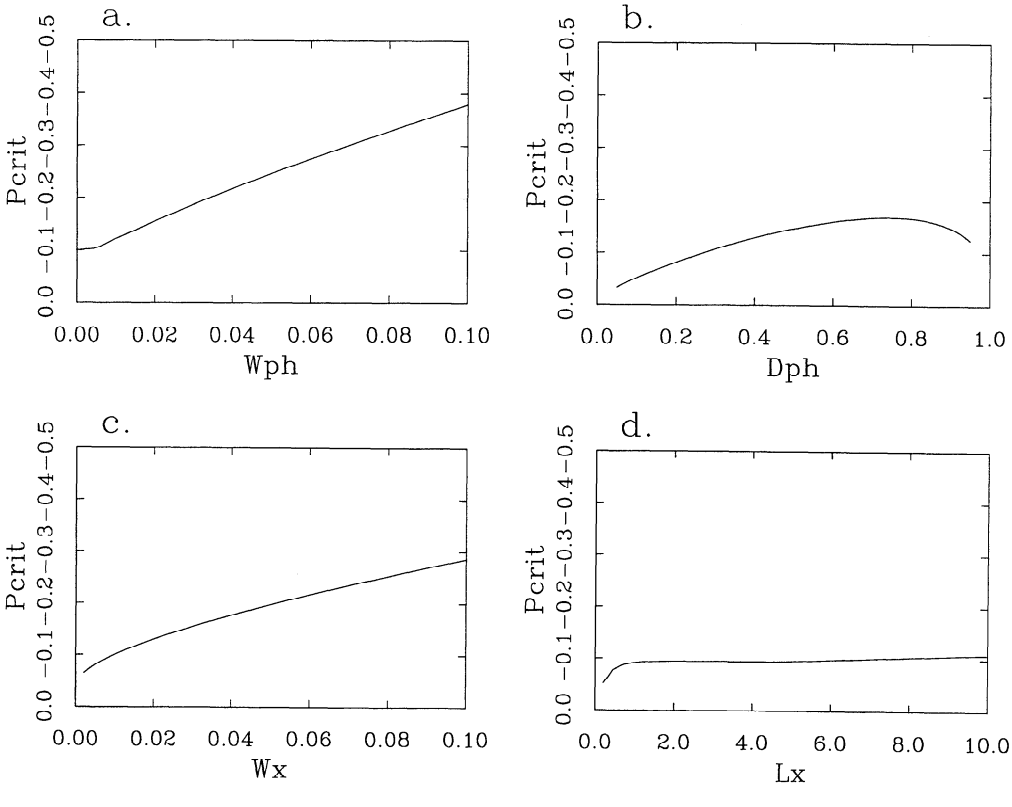

Figure 10. Critical phase buoyancy parameter P_{crit}, plotted against the four important length scales, for internally heated convection with downwellings just reaching the phase transition (Figure 5d).

Discussion and Conclusions

Quantitative values of the critical phase bouyancy parameter P_{crit} have been calculated for a range of scenarios, and the important trends established. Since ponding of upwellings and downwellings at the phase transition is not considered, these values probably represent the threshold between straight penetration of upwellings and downwellings, and an intermittent regime with ponding and avalanches.

In the interaction of upwellings and downwellings with an endothermic phase transition, there are two important lengthscales of the flow: (1) The "outer" wavelength associated with the spacing of upwellings and downwellings and (2) the "inner" wavelength associated with the width of convective features. In general, the long wavelengths associated with the spacing of upwellings and downwellings pass through the phase transition, even when a concentrated feature is deflected at the boundary. This is illustrated in Figure 6, which shows upwellings and downwellings being deflected even though the broad-scale flow penetrates the phase transition. Deflection of an upwelling or downwelling by the phase transition is a short-wavelength mode of flow, and the results here indicate that short wavelengths are more easily deflected than long wavelengths.

From the results presented here, most of the trends observed in numerical simulations of convection with phase transitions (summarized in the introduction) can be explained as a consequence of geometry. These are (1) wavelength dependence of flow penetration, and increased layering due to (2) higher Rayleigh number, (3) internal heating, and (4) narrower phase transitions. These points will now be discussed in detail, together with (5) the effect of phase transition depth and (6) the effect of horizontal wavelength.

1. *Tackley et al.* [1993, 1994] observe in three-dimensional spherical simulations of phase-transition modulated convection that flow penetration through the 670-km phase transition is strongly wavelength dependent, with the longest wavelengths penetrating the phase change easily, but shorter wavelengths becoming increasingly inhibited. The results here with a sinusoidal temperature field provide a direct explanation of this observation. At short wavelengths, only features in the direct vicinity of the "660" influence flow penetration, and there is a proportionality between the phase change strength required to stop flow (P_{crit}), and the wavelength of the flow. Indeed, this proportionality implies that only buoyancy forces that are within a distance to the phase change comparable to the horizontal wavelength matter when considering flow penetration. Thus a more suitable choice of lengthscale to use in the definition of phase buoyancy parameter (equation (5)) would be horizontal wavelength of the feature in question; with this choice, the critical P would always be of order 1. At longer wavelengths, however, features in the entire domain, including boundary conditions, influence the flow, reducing P_{crit} from the value predicted by a proportionally with wavelength.

2. These results show that narrower convective features are more easily deflected and thus result in a greater propensity to layering. This is related to the wavelength dependence of flow penetration observed with sinusoidal anomalies: narrower features have more short-wavelength power than broad features. Since higher Rayleigh numbers lead to narrower features, this implies that higher Rayleigh numbers lead to greater layering, a trend which is well established from numerical simulations [*Christensen and Yuen*, 1985; *Solheim and Peltier*, 1994; *Yuen et al.*, 1994].

Solheim and Peltier [1994] attribute the increase in layering with Rayleigh number to greater temperature anomalies and thus greater phase change deflections. However, it is not clear how this would cause the observed trend, since the important criterion for penetration is the ratio of buoyancy due to phase change deflection to thermal buoyancy, as discussed earlier, and both of these buoyancies increase in proportion to temperature. Thus if phase change deflections and hence temperature anomalies are higher, thermal buoyancy will be higher by the same proportion, and the ratio of the two buoyancy forces is not changed. The results presented here show that greater layering at higher Ra is a natural consequence of geometry, with narrow features being more easily deflected, and does not require any arguments based on temperatures or any other factor. Note, however, that this study does not address the suitability of a local Rayleigh number criterion in determining the breakdown of layered convection [*Solheim and Peltier,* 1994], since this is a different aspect of the system's behavior (compare Figures 1a and 1c).

3. These results indicate that increased internal heating strongly favors greater layering, particularly when the phase change is at a realistic shallow depth. This is consistent with the numerical results of *Zhao et al.* [1992] and *Solheim and Peltier* [1994].

4. *Peltier and Solheim* [1992] demonstrate how layering is enhanced by narrower phase transitions, a trend that was first noted by *Christensen and Yuen* [1985], and is also indicated by the results presented here. The present results also show that the influence of phase transition width is dependent on the horizontal wavelengths, such that short wavelengths are more affected by phase transition width. This suggests that phase transition width is important when it becomes comparable to the width of convective features. Provided the phase transition width is much smaller than convective features, the exact value is not important. However, in most of the numerical simulations currently being performed, phase transition width is comparable to the width of convective features and thus the degree of layering is probably underpredicted.

5. For basally heated convection, the depth of the phase transition does not have a large effect on the overall propensity to layering. This is consistent with the numerical simulations of *Christensen and Yuen* [1985] who note that phase transition depth does not have a strong influence on the critical phase buoyancy parameter. However, when the phase transition is shallower than mid depth, upwellings penetrate more easily than downwellings, consistent with the numerical simulations of *Tackley et al.* [1993, 1994]. Thus for an internally heated mantle, phase transition depth has a large effect on the ability of downwellings to penetrate, such that a shallower phase transition increases the propensity to layering. Since the mantle is thought to be largely internally heated [*Schubert*, 1979; *Davies and Richards*, 1992], it is important to have the phase transition at the correct depth in numerical models, if the results are to be quantitatively correct.

6. *Zhong and Gurnis* [1994] demonstrate using two-dimensional models that with a high viscosity plate subducting as a slab at the end of the box, the degree of layering is strongly affected by the imposed plate length, such that longer lengths favor easier penetration. This may at first appear to contradict the present results, in which horizontal wavelength (L_x) does not significantly affect the dynamics.

However, the surface velocity of the plate in these experiments (which is determined in a dynamically self-consistent manner) only increases by a factor of 2 as the plate length increases by a factor of 5, so that the slabs associated with longer plates are much thicker, as a result of the much longer time for the boundary layer to conductively thicken. Hence upwellings and downwellings are broader and penetrate the endothermic phase transition more easily. Thus the present analysis suggests that the greater penetration observed for longer plates is due to the thicker downwelling slabs, rather than any inherent effect of the horizontal wavelength.

These results have shown that a simple criterion for flow penetration leads to an explanation for all the trends observed in numerical experiments. In the future, it would be useful to apply this model to determine the effects of additional complications. These include three dimensionality, that is, does a cylindrical feature penetrate more or less easily than a linear feature?; the effect of the 400-km phase transition, which acts in the opposite sense to the 660-km phase transition, enhancing the flow of material through itself; the effect of depth-dependent properties associated with compressibility; and the effect of temperature-dependent viscosity, which leads to stronger downwellings and weaker upwellings, thereby influencing flow penetration.

Appendix: Velocity Solution Method

This appendix describes the numerical technique used to obtain velocity solutions. In order to calculate the velocity field associated with a given distribution of buoyancy forces, a spectral technique is used. Variables are expanded using complex Fourier components horizontally (assuming a periodic domain) and a sine or cosine expansion vertically. A vertical sine expansion is used for the stream function ψ and vertical velocity and a cosine expansion for horizontal velocity; for example;

$$\psi(x,z) = \sum_{l,n} \tilde{\psi}_{ln} \exp(-i2\pi lx / A_x)\sin(n\pi z) \tag{23}$$

where A_x is the aspect ratio.

Fourier transforming (23) both horizontally and vertically, we obtain from (6):

$$\tilde{\psi} = \frac{2il}{\pi^3(4l^2+n^2)^2}\tilde{\rho} \tag{24}$$

and hence the velocity components

$$\tilde{u} = -\frac{2inl}{\pi^2(4l^2+n^2)^2}\tilde{\rho} \tag{25}$$

$$\tilde{v}_z = 2\pi il\tilde{\psi} = \frac{4l^2}{\pi^2(4l^2+n^2)^2}\tilde{\rho}. \tag{26}$$

Thus the numerical technique is very straightforward, consisting of (1) transforming the density distribution into (ℓ,n) space using fast Fourier transforms, (2) multiplying the density coefficients by the above factors to get velocity coefficients, then (3) transforming velocities back into grid space. This method is very efficient computationally and can be accomplished on a Sun Sparcstation 2 workstation, even with hundreds of points in each direction.

As with the infinite domain case derived analytically in the main text, solutions for thermally driven flow and phase-change driven flow are calculated separately. Using the linearity of the instantaneous velocity solution, the critical phase buoyancy parameter required for zero flow across the phase boundary is obtained.

Table 3. Convergence Test for Standard Problem

Resolution		Spectral Drop-Off (Orders of Magnitude)		
nx	nz	x	z	P_{crit}
1024	1025	21.7	12.6	-0.165803
512	513	19.6	10.8	-0.166254
256	257	8.35	9.01	-0.165460
128	129	4.83	7.23	-0.166257
64	65	3.60	6.10	-0.181275

Some of the density distributions considered, such as the sheet mass anomaly (a delta function in z), do not have a convergent spectral representation. However, we are interested in the velocity field and, as can be seen above, the spectral coefficients for velocity drop off asymptotically as n^{-3} or n^{-4} for a delta function density anomaly, and thus the velocity field can be well resolved with relatively few harmonic coefficients, even if the density field cannot.

To test the number of vertical and horizontal components required, convergence tests have been performed for the standard case of stopped Gaussian anomalies of half width 0.01 in a periodic (in x) domain of period 2, sheet mass anomaly phase change at 0.25 depth. The calculated value of P_{crit} is tabulated in Table 3 for various resolutions. In the cases reported, a resolution of 128x129 is typically used, giving an accuracy for P_{crit} of better than one part in 10^3.

Acknowledgments. The author thanks David Bercovici and Ulrich Christensen for helpful reviews of the manuscript, and David Stevenson and Shixjie Zhong for thoughtful comments and corrections, respectively. Supported by NSF grant EAR9017893. Caltech Division of Geological and Planetary Sciences contribution 5441.

References

Benz, H.M., and J.E. Vidale, Sharpness of upper-mantle discontinuities determined from high-frequency reflections, *Nature, 365*, 147-150, 1993.

Bercovici, D., G. Schubert, and P.J. Tackley, On the penetration of the 660 km phase change by mantle downflows, *Geophys. Res. Lett., 20*, 2599-2602, 1993.

Christensen, U.R., and D.A. Yuen, Layered convection induced by phase transitions, *J. Geophys. Res., 90*, 10291-10300, 1985.

Davies, G.F., and M.A. Richards, Mantle convection, *J. Geol., 100*, 151-206, 1992.

Gradshteyn, I.S., and I.M. Ryzhik, *Table of Integrals, Series, and Products*, edited by A. Jeffrey, 1160 pp., Academic, San Diego, Calif., 1980.

Honda, S., D.A. Yuen, S. Balachandar, and D. Reuteler, Three-dimensional instabilities of mantle convection with multiple phase transitions, *Science, 259*, 1308-1311, 1993.

Ito, E., and E. Takahashi, Postspinel transformations in the system Mg_2SiO_4-Fe_2SiO_4 and some geophysical implications, *J. Geophys. Res., 94*, 10637-10646, 1989.

Liu, M., D.A. Yuen, W. Zhao, and S. Honda, Development of diapiric

structures in the upper mantle due to phase transitions, *Science, 252*, 1836-1839, 1991.

Machetel, P., and P. Weber, Intermittent layered convection in a model mantle with an endothermic phase change at 670 km, *Nature, 350*, 55-57, 1991.

Peltier, W.R., and L.P. Solheim, Mantle phase transitions and layered chaotic convection, *Geophys. Res. Lett., 19,* 321-324, 1992.

Peltier, W.R., G.T. Jarvis, A.M. Forte, and L.P. Solheim, The radial structure of the mantle general circulation, in *Mantle Convection: Plate Tectonics and Global Dynamics,* edited by W.R. Peltier, pp. 765-816, Gordon and Breach, New York, 1989.

Phipps Morgan, J., and P.M. Shearer, Seismic constraints on flow and discontinuity topography near 660 km - New evidence for whole mantle convection, *Nature*, *365*, 506-511, 1993.

Schubert, G., Subsolidus convection in the mantles of terrestrial planets, *Annu. Rev. Earth Planet. Sci., 7*, 289-342, 1979.

Schubert, G., and D.L. Turcotte, Phase transitions and mantle convection, *J. Geophys. Res., 76*, 1424-1432, 1971.

Schubert, G., D.A. Yuen, and D.L. Turcotte, Role of phase transitions in a dynamic mantle, *Geophys. J. R. Astron. Soc., 42*, 705-735, 1975.

Solheim, L.P., and W.R. Peltier, Avalanche effects in phase transition modulated thermal convection: A model of the Earth's mantle, *J Geophys. Res., 99*, 6997-7018, 1994.

Tackley, P.J., D.J. Stevenson, G.A. Glatzmaier, and G. Schubert, Effects of an endothermic phase transition at 670 km depth in a spherical model of convection in the Earth's mantle, *Nature, 361*, 699-704, 1993.

Tackley, P.J., D.J. Stevenson, G.A. Glatzmaier, and G. Schubert, Effects of multiple phase transitions in a three-dimensional spherical model of convection in Earth's mantle, *J. Geophys. Res., 99,* 15877-15901, 1994.

Turcotte, D.L., and G. Schubert, *Geodynamics: Applications of Continuum Physics to Geological Problems*, 450 pp, John Wiley, New York, 1982.

Weinstein, S.A., Catastrophic overturn of the Earth's mantle driven by multiple phase changes and internal heat generation, *Geophys. Res. Lett., 20*, 101-104, 1993.

Yuen, D.A., and P. Olson, Thermochemical plumes and mantle phase transitions, *J. Geophys. Res., 87*, 3993-4002, 1982.

Yuen, D.A., D.M. Reuteler, S. Balachandar, V. Steinbach, A.V. Malevsky, and J.J. Smedsmo, Various influences on 3-dimensional mantle convection with phase transitions, *Phys. Earth Planet. Inter., 86*, 185-203, 1994.

Zhao, W., D.A. Yuen, and S. Honda, Multiple phase transitions and the style of mantle convection, *Phys. Earth Planet. Inter., 72* , 185-210, 1992.

Zhong, S., and M. Gurnis, Role of plates and temperature-dependent viscosity in phase change dynamics, *J. Geophys. Res., 99,* 15903-15917, 1994.

P. J. Tackley, Department of Earth and Space Sciences, University of California Los Angeles, Los Angeles, CA 90024. (e-mail: ptackley@ess.ucla.edu)

(Received August 17, 1994; revised January 17, 1995;
accepted January 26, 1995.)